ACS central science

http://pubs.acs.org/journal/acscii

Research Article

High-Voltage Aqueous Redox Flow Batteries Enabled by Catalyzed Water Dissociation and Acid−Base Neutralization in Bipolar Membranes

Zhifei Yan, Ryszard J. Wycisk, Amy S. Metlay, Langqiu Xiao, Yein Yoon, Peter N. Pintauro, and Thomas E. Mallouk*

Cite This: *ACS Cent. Sci.* 2021, 7, 1028−1035

Read Online

ACCESS | Metrics & More | Article Recommendations | Supporting Information

ABSTRACT: Aqueous redox flow batteries that employ organic molecules as redox couples hold great promise for mitigating the intermittency of renewable electricity through efficient, low-cost diurnal storage. However, low cell potentials and sluggish ion transport often limit the achievable power density. Here, we explore bipolar membrane (BPM)-enabled acid−base redox flow batteries in which the positive and negative electrodes operate in the alkaline and acidic electrolytes, respectively. This new configuration adds the potential arising from the pH difference across the membrane and enables an open circuit voltage of ∼1.6 V. In contrast, the same redox molecules operating at a single pH generate ∼0.9 V. Ion transport in the BPM is coupled to the water dissociation and acid−base neutralization reactions. Interestingly, experiments and numerical modeling show that both of these processes must be catalyzed in order for the battery to function efficiently. The acid−base concept provides a potentially powerful approach to increase the energy storage capacity of aqueous redox flow batteries, and insights into the catalysis of the water dissociation and neutralization reactions in BPMs may be applicable to related electrochemical energy conversion devices.

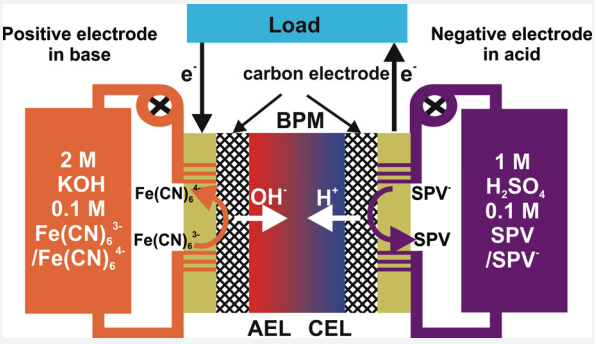

INTRODUCTION

The intermittent nature of renewable energy sources such as solar and wind presents a barrier to their large-scale implementation, a problem that can potentially be addressed by an efficient and cost-effective means of electrical energy storage over periods of days. Electrochemistry provides a viable solution to the problem by storing charge that can be converted back to electrical power with high round-trip efficiency.[1,2] Among electrochemical energy storage devices, aqueous redox flow batteries are promising because of the vast design space of redox molecules, the independence of energy and power density, the scalability of energy storage, and the manufacturability of cell hardware. To compete with alternative storage methods, however, improvements in energy and power density, cell lifetime, cost, and safety are still needed.[3−5]

A higher battery potential increases the power density of redox flow batteries, which in turn reduces the stack cost.[5] Increasing the cell potential has so far been achieved mainly by designing redox molecules with more extreme redox potentials,[4,6−9] but the factors of reversibility, solubility, and raw materials availability must be considered for practical large-scale usage. The creation of a cross-membrane potential by means of pH gradient can add to the potential difference between the redox molecules, providing a simple tool for increasing the cell potential. This idea has been studied with water electrolysis at the anode and cathode, but the high overpotentials of the water oxidation and oxygen reduction reactions compromise the efficiency of energy storage.[10−12] The use of a pH gradient to increase the voltage of a primary battery based on flowing redox molecules has been studied in microfluidic devices by generating a laminar flow of acidic and basic solutions.[13,14] For this approach to scale to macroscopic dimensions, a membrane is needed to maintain the pH gradient while transporting ions that charge-compensate the anode and cathode reactions. Here we exploit the fact that bipolar membranes (BPM), composed of a cation exchange layer (CEL) and an anion exchange layer (AEL), can effectively manage the transport of proton and hydroxide ions while maintaining a stable pH gradient at high current densities.[15−17] In contrast to conventional acidic or alkaline redox flow batteries that operate at a single pH, the BPM-

Received: February 16, 2021
Published: May 28, 2021

enabled acid−base redox flow battery places the positive and negative electrodes in high and low pH environments, respectively (Figure 1a).

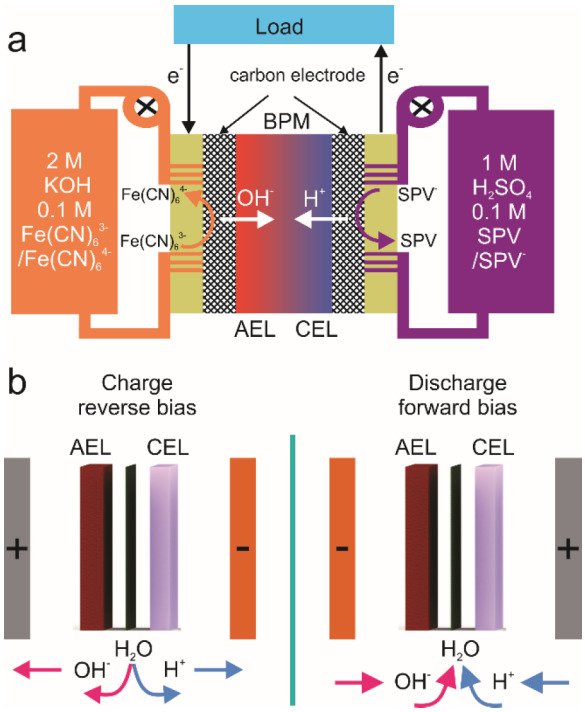

Figure 1. Schematic illustration of a BPM-based acid−base redox flow battery. (a) The discharging process of the battery is shown, where ferrocyanide ($Fe(CN)_6^{4-}$) in aqueous KOH is reduced and SPV (sulfonatopropyl viologen, structure shown in Figure 3a) in H_2SO_4 is oxidized at the positive and negative electrodes, respectively. The H^+ and OH^- ions carry the charge in the bipolar membrane (BPM) that is composed of anion- and cation- exchange layers (AEL and CEL). The electrolytes are cycled through the cell using a peristaltic pump. (b) The transport of H^+ and OH^- ions is coupled with the water dissociation and acid−base neutralization reactions during the charging and discharging processes, respectively. The AEL and CEL face the positive and negative electrodes, respectively. The BPM is subject to reverse bias when the flow battery is charging and operates in forward bias during discharge.

The functioning of an acid−base redox flow battery relies on matching operating pH's with the properties of the redox molecules, as well as effective ion management in the membrane electrolyte. A successful design must consider the stability of materials,[18,19] the pH-dependent reaction kinetics,[20−22] and the pH-dependent shifts in redox potentials.[15] The fast kinetics of the H_2/H^+ and O_2/OH^- half reactions in acidic and basic media, respectively, have motivated the study of BPMs in H_2-O_2 fuel cells[20] and water electrolyzers,[15,23,24] where the thermodynamic potential of the overall reaction is unchanged because the membrane potential is matched by the Nernstian shift of the redox reactions. Previous efforts to use the membrane potential as an independent element of energy storage have been compromised by the lack of reversible redox processes at the electrodes, resulting in a low system round-trip efficiency.[12,25]

To achieve high energy conversion efficiency, effective management of ion transport is also required as ions carry the current in the electrolyte. The transport of H^+ and OH^- is coupled with the water dissociation and acid−base neutralization reactions at the AEL/CEL interface, which acts as a source or sink of ions in the charging and discharging processes, respectively (Figure 1b). Water dissociation is a slow process, but it can be accelerated by an applied electric field, which creates an overpotential for the charging reaction and by interfacial catalysis at the AEL/CEL junction.[17,26] Acid−base neutralization in forward bias, on the other hand, is generally thought to be rapid and so has received less attention. A previous numerical simulation proposed a trap-assisted charge recombination mechanism for H^+ and OH^- in acid−base fuel cells.[21] More detailed experiments and simulations, which we present below, provide further insight into free energy losses associated with this key process.

The neutralization reaction of H^+ and OH^- is rate-limited by their local concentrations in the region of the CEL/AEL interface. As a result, much of the potential generated across the BPM by the pH gradient can be lost when a forward bias is applied, unless the AEL/CEL interface is equipped with a suitable catalyst, such as graphene oxide (GO), to maintain the quasi-equilibrium of H^+, OH^-, and water. Understanding these effects enables us to successfully demonstrate a reversible BPM-based acid−base redox flow battery that achieves a ∼1.6 V cell potential using the same redox molecules (ferrocyanide and a viologen derivative), which, operating at a single pH, create only a ∼0.9 V overall potential.

RESULTS AND DISCUSSION

BPM under Forward Bias. The BPM plays an important role in the acid−base redox flow battery because it separates the positive and negative electrodes, prevents crossover of redox molecules, and conducts ions. The BPM is composed of a sulfonated poly(ether ether ketone) (SPEEK) CEL, GO as interfacial catalyst, and AEL (30 μm, Fumasep FAS-30). To study the BPM in isolation, we monitored the cross-membrane potential by using a four-electrode setup (Figure 2a), which eliminates the influence of the redox processes on the electrodes.[17] 0.1 M KOH and 0.1 M HCl solutions were placed on the AEL and CEL sides of the BPM, respectively, creating a pH gradient with an open circuit potential of ∼710 mV (Figure 2d). The BPM containing an interfacial GO catalyst layer had a smaller overpotential under both reverse- and forward-bias conditions. The difference in the overpotential reflects the acceleration of reaction rates by GO at the AEL/CEL interface since the potentials were corrected for ohmic resistance. Slower reaction kinetics in BPMs without catalyst were confirmed by electrochemical impedance spectroscopy (EIS) measurements (Figure S1). It is interesting to note that the presence of the GO catalyst also significantly affects the acid−base neutralization process (Figure 2d), even though the rate of that reaction is typically assumed to be diffusion-controlled in liquid water.

To gain more insight into the effect of the catalyst, we constructed a one-dimensional numerical model with four segments representing the basic and acidic electrolytes separated by the AEL and CEL of a BPM (Figure 2b). A potential difference was imposed on the two open boundaries that act as the reference electrodes, and the current density was collected based on the ionic fluxes. To study the influence of the catalyst on the rates of the dissociation (k_d) and neutralization (k_n) processes, we compared three models that differed in their expressions for k_d and k_n. The experimental BPM without GO catalyst was represented by a constant k_d and k_n throughout all the domains, denoted Model 1

https://doi.org/10.1021/acscentsci.1c00217
ACS Cent. Sci. 2021, 7, 1028−1035

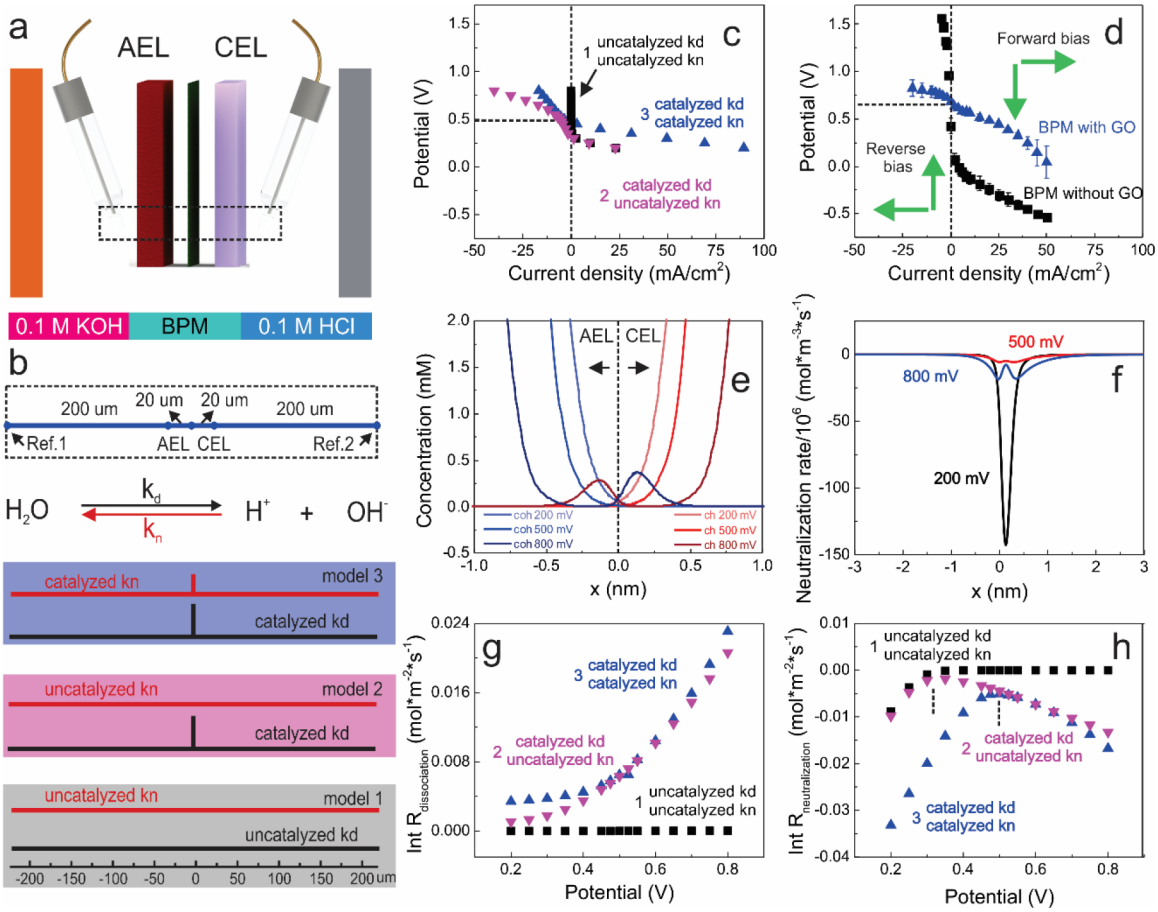

Figure 2. The effects of interfacial catalysis in the BPM. (a) The experimental four-electrode setup for measuring the potential drop across the BPM. Using two reference electrodes eliminates the influence of the electrochemical reactions at the electrodes. KOH and HCl are used as the electrolytes on the AEL and CEL sides, respectively, of the BPM. The dashed box represents the region of interest that was modeled in numerical simulations. (b) The experimental setup was simplified as a one-dimensional model that includes four segments and two open boundaries (dashed box). This region corresponds to the region in (a). To explore the effect of catalysis on the potential−current density relation under reverse- and forward-bias conditions, we compared three models. Model 1 simulates the experimental BPM without a catalyst, imposing constant k_d and k_n. Models 2 and 3 assume the presence of a catalyst layer at the AEL/CEL interface, which increases k_d by three orders of magnitude; the neutralization rate constant k_n is also increased by the catalyst in Model 3 but not in Model 2. (c) Cross-membrane potential−current density curves from the three models, compared to the experimental results shown in (d). Only Model 3 with catalyzed k_d and catalyzed k_n can reproduce the trends observed in BPMs with and without catalyst layers (GO, graphene oxide) under both reverse and forward bias. The dashed lines indicate the open circuit condition. Error bars represent the standard deviation of three independent measurements. (e) Concentration profiles of H^+ and OH^- near the AEL/CEL interface (Model 3). The neutralization reaction is rate-limited by the negligible amount of either H^+ or OH^- in the AEL/CEL, resulting in a narrow reaction zone as shown in (f). (g) The integrated reaction rate of the dissociation and (h) neutralization processes over the reaction zone. The neutralization rate increases to a maximum under a small reverse bias, even though the net reaction at that point is water dissociation. The dashed lines indicate the open circuit condition for Models 2 and 3.

uncatalyzed k_d/uncatalyzed k_n. For BPMs with an interfacial GO layer, a spacing of 20 nm at the AEL/CEL interface was assumed to be occupied by the catalyst. This approach further assumes that the presence of the catalyst increased the value of k_d by three orders of magnitude. In two other models, the neutralization kinetics were either unaffected or increased by the presence of the interfacial catalyst, corresponding to Model 2 catalyzed k_d/uncatalyzed k_n, and Model 3, catalyzed k_d/catalyzed k_n, respectively. It should be pointed out that Model 2 is nonphysical (but still instructive, *vide infra*) because a catalyst for water dissociation must also catalyze the reverse reaction. In this regard, Model 2 effectively shifts the thermodynamics of the reaction to favor the dissociation direction. Comparison of the computational and experimental results shows that even though catalyzing k_d alone is sufficient to reproduce the overpotential difference under reverse bias (Model 2), the higher current densities obtained in the BPM with GO at a given forward bias are reproduced only when both k_d and k_n are catalyzed (Model 3) (Figure 2c,d).

We next sought to quantify the local concentrations of the species (OH^-, H^+, and H_2O) involved in the dissociation and neutralization processes in BPMs. The ion distribution profiles reveal high concentrations of OH^- and H^+ inside the AEL and CEL but negligible amounts of co-ions K^+ and Cl^- as 100% permselectivity was assumed for the ion exchangers (Figure S2). Diffusion boundary layers at the membrane/aqueous electrolyte interface can also be seen under both reverse and forward polarizations.[27] The thickness of the depletion layer at the AEL/CEL interface decreases as more ions are driven into the membrane under forward bias (Figure S2b).[21] The depletion layer also causes most of the potential drop to be in the junction region (Figure S3). A key point is that the

https://doi.org/10.1021/acscentsci.1c00217
ACS Cent. Sci. 2021, 7, 1028−1035

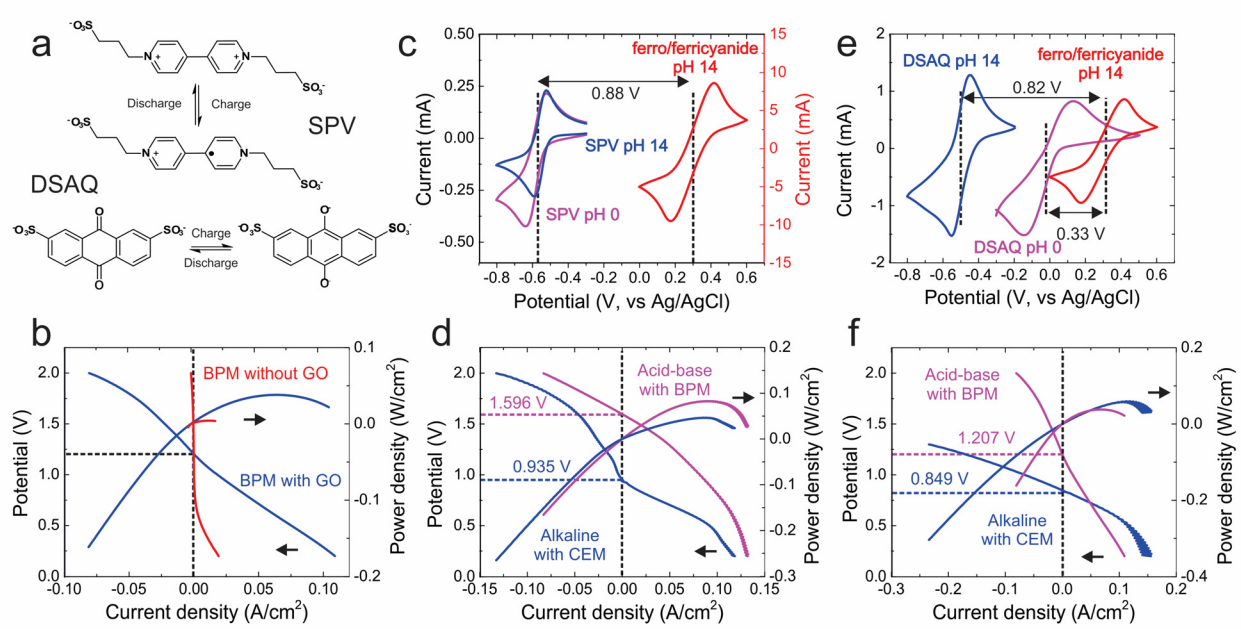

Figure 3. Performance of the acid−base redox flow battery. (a) Structures of the redox couples used at the negative electrode. SPV: 1,1′-bis(3-sulfonatopropyl)-4,4′-bipyridinium, DSAQ: 2,7-difulfonate-9,10-anthroquinone. 0.1 M ferrocyanide in 2 M KOH was used as the positive electrolyte for all the cell performance tests. (b) Cell performance with and without GO as the catalyst in the BPM. Improved performance can be achieved using BPMs with GO due to the increased dissociation and neutralization rate constants. Electrolyte: 0.1 M DSAQ (1 M H_2SO_4) in the negative electrolyte. (c) Cyclic voltammogram (CV) of 0.1 M SPV in 1 M H_2SO_4 (magenta) or in 1 M KOH (blue), and 0.5 M ferrocyanide in 1 M KOH (red); and (e) CV of 0.1 M DSAQ in 1 M H_2SO_4 (magenta) or in 1 M KOH (blue) and 0.1 M ferrocyanide in 1 M KOH (red). The SPV redox couple is pH-independent, whereas the formal potential of DSAQ shifts positively at lower pH. (d, f) Potential and power density versus current density curves at ∼100% state of charge. With the common positive electrode, operating SPV in acid (acid−base with BPM) increases the cell potential by ∼0.66 V compared to a cell operated under a single alkaline condition (alkaline with CEM). The same comparison with the DSAQ redox couple shows an ∼0.35 V increase in the cell potential.

neutralization reaction requires the presence of *both* OH^- and H^+ ions, most of which, however, are spatially confined by the immobilized charge in the bulk of the AEL and CEL (Figure 2e). The overlap of these two species is limited to a narrow region at the AEL/CEL interface, where the concentration of the major charge carrier (OH^- for AEL and H^+ for CEL) decreases rapidly in the direction of the other ion exchanger (CEL and AEL) (Figure 2e). Significant reaction rates of dissociation and neutralization are found only in a region of ∼2−3 nm thickness (the reaction zone) (Figures 2f and S4). The diffusional transport of OH^- and H^+ into the CEL and AEL, respectively, is balanced by the electrostatic force at the open circuit; further penetration, and thus a higher reaction rate, would require the application of an increased forward bias (Figure 2f). There should be negligible polarization loss due to the low concentration of ionic species at the AEL/CEL interface because of the extreme thinness of the junction region.

To explore the effect of catalysis, we compared the integrated reaction rates of the dissociation and neutralization processes over the reaction zone for the three different models. The dissociation rate increases monotonically as the applied potential increases, which also results in an increase in the electric field (Figures 2g and S5). The neutralization rate decreases to a minimum around the open circuit potential (∼300/500 mV for Models 2/3) and increases under reverse bias (Figure 2h). Models 2 and 3 with catalyzed k_d exhibit larger dissociation rates over the whole potential range, as well as an accelerated neutralization rate even with an uncatalyzed k_n (Model 2) under reverse bias. The net reaction in the reverse-biased BPM (800 mV, Figure 2e) is water dissociation as evidenced by the changes in water concentration (Figure S6), but it produces the rate-limiting species OH^- and H^+ in the CEL and AEL, respectively, which in turn intensifies the neutralization reaction. The correlation between the two reactions also suggests the important role of water, which is sufficient when aqueous electrolytes are used but might become a limiting factor in water-vapor fed devices such as H_2-O_2 fuel cells.[14] Increasing the catalytic acceleration to more than three orders of magnitude induces relatively smaller current changes in forward bias relative to that seen in reverse bias (Figure S7).

With the reaction zone for neutralization limited to the nanoscale region in which both reactants are present, mechanisms that effectively increase the local concentration elsewhere should increase the overall reaction rate. By assuming the presence of trap states in the bulk of the membrane, a trap-assisted recombination process was proposed that theoretically predicted a 4−5 orders of magnitude higher achievable current density than in the case without traps.[21] The mechanism by which the GO catalyst in the experimental BPM increases the acid−base neutralization reaction remains unknown and requires further investigation, but the study of the opposite process (dissociation) has recently received significant attention and could potentially provide useful insight.[26,28] The results of molecular dynamics simulations of the water autodissociation and proton transfer processes in free water can be instructive in understanding the dissociation and neutralization reactions in BPMs.[29,30] Water dissociation is proposed to be initiated by the local electric

https://doi.org/10.1021/acscentsci.1c00217
ACS Cent. Sci. 2021, 7, 1028−1035

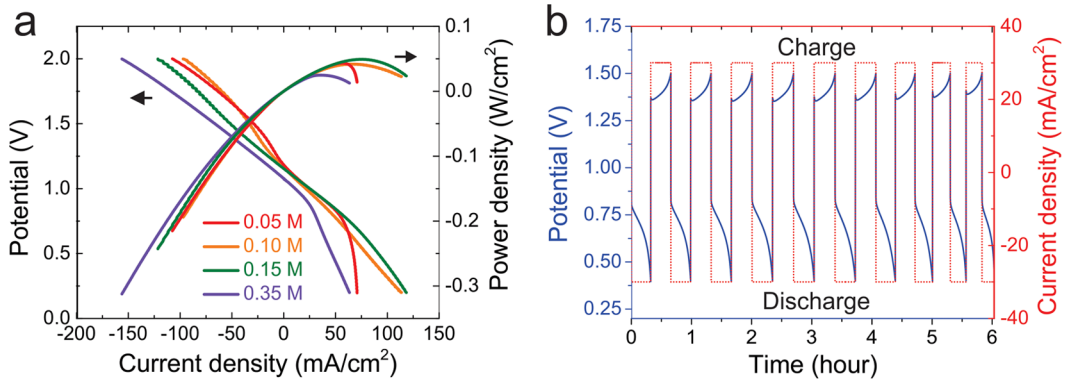

Figure 4. Cell performance at different concentrations of ferrocyanide and a cycling test. (a) Polarization and power density curves of cells operating at different concentrations of ferrocyanide in 2 M KOH; a negative electrolyte of 0.4 M DSAQ in 1 M H_2SO_4 was used. The best cell performance was observed at intermediate concentrations (0.15 M). (b) Potential and current density versus time during the first 10 charge–discharge cycles. Positive electrolyte: 6 mL of 0.1 M $K_4Fe(CN)_6$ in 2 M KOH; negative electrolyte: 6 mL of 0.1 M DSAQ in 1 M H_2SO_4; charging and discharging at 30 mA/cm^2.

field arising from solvation fluctuations. The separation of the nascent H^+/OH^- pair is further assisted by solvent-generated electric fields that also accompany the recombination of hydronium and hydroxide ions. It is thus not surprising that the dissociation and recombination events are affected by electric fields. The second Wien effect accounts for the presence of unbalanced fixed charge and electric field in the depletion layer, which perturbs the equilibrium between water, H^+ and OH^-. It should also be noted that the chemical environment of the BPMs, particularly near the AEL/CEL interface, may alter the reaction mechanisms relative to their counterparts in free water. For example, water molecules within the BPM junction region are considered more ordered and dielectrically saturated than in free water, leading to a smaller dielectric constant.

BPM-Based Acid–Base Redox Flow Battery. On the basis of our understanding of the catalyzed acid–base neutralization process, we explored the incorporation of a BPM-based pH gradient into a conventional redox flow battery. Cell testing was conducted at room temperature by dissolving potassium ferrocyanide in 2 M KOH as the positive electrode and either the electroneutral viologen derivative SPV or 2,7-difulfonate-9,10-anthroquinone (DSAQ) (Figure 3a) in 1 M H_2SO_4 as the negative electrode (Figure 1a). The electrolytes were separated by a BPM with the AEL/CEL facing the positive/negative sides, respectively. The polarization results were collected after applying a charging current of 30 mA/cm^2 to reach ∼100% state of charge. Incorporating a GO catalyst into the BPM results in significantly improved cell performance for both the charging and discharging process (Figure 3b) because of the enhanced dissociation and neutralization kinetics as discussed above (Figure 2d).

To successfully harness the pH-derived cross-membrane potential in the acid–base redox flow battery, pH-independent redox couples are desired as the voltage gain due to the pH gradient could be offset by Nernstian shifts in the formal potentials of the molecules. To illustrate this concept, we compared two redox reactions that had distinct dependences on the pH at the negative electrode. The formal potential of the SPV redox couple is unaffected by pH (Figure 3c), whereas that of DSAQ shifts positively as the pH changes from 14 to 0 (Figure 3e). When coupled with ferrocyanide in base as the positive redox couple, SPV operating in acid results in an open circuit voltage of ∼1.6 V, whereas a single alkaline condition gives only ∼0.94 V using the same redox pair (Figure 3d). The acid–base configuration therefore retains a large portion (∼0.66 V) of the pH-derived cross-membrane potential (theoretically 0.83 V). In comparison, the cell with DSAQ shows only a ∼0.35 V potential increase (Figure 3f), with the remaining potential being lost due to the positive shift of the negative electrode in acid.

The polarization test showed significant mass transport limitation at high current density during the discharging process. We thus carried out EIS measurements of the full cell in order to understand the impedance losses due to various processes. The EIS results indicated that impedance losses are associated with the series resistance (high frequency, ∼10^5 Hz), the reaction kinetics inside the BPMs (intermediate frequency, ∼10^3 Hz), and mass transport (low frequency, ∼0.1 Hz) (Figure S8). When the concentration of redox molecules is low (0.05 M), the mass transport resistance increases under high forward bias, whereas changes in the dissociation and neutralization kinetics at the AEL/CEL interface are insignificant. On the other hand, more concentrated redox couples (0.3 M) lead to a slower neutralization process (Figure S9) because the negatively charged $Fe(CN)_6^{4-}$/ $Fe(CN)_6^{3-}$ species tends to compete with the charge carrier OH^- for sites in the AEL, limiting the amount of OH^- that is available for the neutralization reaction. It could also be affected by the presence of K in BPM under forward bias (see below). A balance between the kinetic and transport resistance is achieved at intermediate concentrations (0.1 and 0.15 M, Figure S10), resulting in the best discharging performance (Figure 4a). Designing stable and positively charged redox couples for the positive side of the flow battery is thus a promising avenue for improving device performance.[31−33]

Preliminary charging–discharging tests with the DSAQ and $K_4Fe(CN)_6$ showed performance degradation after 10 cycles (Figure 4b, specific charging and discharging curves in Figure S11), and understanding the origin of the degradation will be useful for improving long-term stability. The cyclability of the battery depends on the chemical stability and crossover rates of the redox couples, as well as the durability of BPMs. We first considered the latter. Stability tests of BPMs under reverse bias (charging process) have been done,[17,26,34] but there are limited demonstrations of stable BPMs operating under forward bias. Because of the nonideal permselectivity of BPMs and possible crossover of acid and base under operating conditions, we

https://doi.org/10.1021/acscentsci.1c00217
ACS Cent. Sci. 2021, 7, 1028−1035

monitored the cross-membrane potentials under repetitive reverse- and forward-bias cycles, mimicking the operation of the BPM in the flow battery. There was slight increase (<30 mV) in the overpotential after 10 cycles (Figure S12a), which was not significant enough to explain the performance degradation in the flow battery tests. The open circuit voltage (OCV) remained unchanged during a 12-h test, suggesting negligible crossover of acidic and basic electrolytes (Figure S12b). After a significant performance decrease was observed in the flow battery, we measured the cross-membrane potential of the BPM under both reverse and forward biases. Compared with the BPM before battery testing, a minimal difference in the polarization curves was observed (Figure S13). Interestingly, adding $K_3Fe(CN)_6$ to the positive electrolyte does not affect the reverse bias regime but decreases the forward limiting current density to below 30 mA/cm^2, compared to >100 mA/cm^2 in the original sample (Figure S13). This can be explained by the fact that under reverse bias, $Fe(CN)_6^{4-}$/$Fe(CN)_6^{3-}$ anions migrate away from the AEL to the positive electrode, while under forward bias they are driven into the AEL and affect the acid−base neutralization process, which is consistent with the EIS results discussed above. Photographs of the BPMs before and after battery testing showed apparent color changes (Figure S14), either due to the absorption of redox species or the color charge of the AEL upon exposure to the alkaline electrolyte. ICP-OES measurements (Table 2, Supporting Information) showed significant amounts of Fe and K in the BPM as well as in the negative electrolyte, after the battery tests. This further supports the hypothesis that the absorption of redox species into the AEL of the BPM interferes with the acid−base neutralization reaction. The influence of the side reaction of water splitting is significant only at high cell potentials (>2 V, Figure S15), which is above the charging limits of our tests. Asymmetric pH conditions have been studied using designs similar to desalination electrodialysis in which the AEM and CEM are separated by macroscopic electrolyte layers.[35,36] In this configuration, the charge carriers are the counterions of the acid and base (K^+ and Cl^- for KOH and HCl), and the interfacial electric field vanishes due to the large separation between the two membranes.

CONCLUSIONS

An acid−base redox flow battery was developed using a BPM that enables the positive and negative electrodes to operate under alkaline and acidic conditions, respectively. The creation of a stable pH gradient allows the cross-membrane potential to be added to the formal potential differences of the redox molecules, resulting in a substantially increased cell potential relative to the same molecules at a single pH. The transport of H^+ and OH^- is coupled to the water dissociation and acid−base neutralization process at the AEL/CEL interface in the BPM. Through a combined experimental and numerical simulation study, we found that the rate-limiting factor in the acid−base neutralization reaction is the concentration of minority ions (H^+ for AEL and OH^- for CEL), and equipping the interface with a catalyst significantly increases the reaction rate, resulting in higher discharging performance of the redox flow battery.

This study has demonstrated the principle by which a bipolar membrane-based redox flow battery can achieve higher voltage and thus higher energy storage capacity. This was shown at the proof-of-concept level by using off-the-shelf redox couples (ferro-/ferricyanide and SPV) that are not indefinitely stable in the flow battery environment; for example, ferricyanide is subject to slow decomposition in strong base, and SPV is air-sensitive in its reduced forms. In addition, ion pairing of K^+ with ferro-/ferricyanide ions results in crossover of K^+ ions, which compromises the cycle life of the BPM-based redox flow battery. Designing stable redox molecules that are compatible with the acid−base environment and the electrostatic charges in the AEL/CEL is a remaining challenge, and such redox couples could also lead to higher power redox flow batteries. The long-term stability of the flow battery also requires stable operation of BPMs under forward-bias conditions and minimal species crossover, which depends on the size, charge, and pH of the electrolyte,[37] as well as the pore size and charge distribution of the membranes.[38−40]

ASSOCIATED CONTENT

Supporting Information

The Supporting Information is available free of charge at https://pubs.acs.org/doi/10.1021/acscentsci.1c00217.

Details of the experiments and numerical modeling, electrochemical impedance spectra, stability of BPMs, and ICP-OES data (PDF)

AUTHOR INFORMATION

Corresponding Author

Thomas E. Mallouk − *Department of Chemistry, University of Pennsylvania, Philadelphia, Pennsylvania 19104, United States*; orcid.org/0000-0003-4599-4208; Email: mallouk@sas.upenn.edu

Authors

Zhifei Yan − *Department of Chemistry, University of Pennsylvania, Philadelphia, Pennsylvania 19104, United States*

Ryszard J. Wycisk − *Department of Chemical and Biomolecular Engineering, Vanderbilt University, Nashville, Tennessee 37235, United States*

Amy S. Metlay − *Department of Chemistry, University of Pennsylvania, Philadelphia, Pennsylvania 19104, United States*

Langqiu Xiao − *Department of Chemistry, University of Pennsylvania, Philadelphia, Pennsylvania 19104, United States*; orcid.org/0000-0003-0695-3075

Yein Yoon − *Department of Chemistry, University of Pennsylvania, Philadelphia, Pennsylvania 19104, United States*

Peter N. Pintauro − *Department of Chemical and Biomolecular Engineering, Vanderbilt University, Nashville, Tennessee 37235, United States*

Complete contact information is available at: https://pubs.acs.org/10.1021/acscentsci.1c00217

Author Contributions

Z.Y., P.N.P., and T.E.M. designed the study. Z.Y. carried out the experimental work and numerical simulations with assistance from A.S.M., and Y.Y. calculated Pourbaix diagrams for candidate redox couples. R.J.W. prepared the SPEEK CEL solution, and L.X. assisted in the preparation of the redox molecules. Z.Y. and T.E.M. drafted the manuscript, which was reviewed and edited by all authors.

Notes

The authors declare no competing financial interest.

■ ACKNOWLEDGMENTS

We thank Dr. David R. Vann for assisting with the ICP-OES measurements. This work was primarily supported by the Center for Alkaline-Based Energy Solutions, an Energy Frontier Research Center program supported by the U.S. Department of Energy, under Grant DE-SC0019445. The work performed at Vanderbilt University was supported by the ARPA-E, Award No. DE-AR0001035. Y.Y. acknowledges summer support from the Vagelos Integrated Program in Energy Research at the University of Pennsylvania.

■ REFERENCES

(1) Lewis, N. S.; Nocera, D. G. Powering the Planet: Chemical Challenges in Solar Energy Utilization. *Proc. Natl. Acad. Sci. U. S. A.* **2006**, *103* (43), 15729−15735.
(2) Yan, Z.; Hitt, J. L.; Turner, J. A.; Mallouk, T. E. Renewable Electricity Storage Using Electrolysis. *Proc. Natl. Acad. Sci. U. S. A.* **2020**, *117*, 12558.
(3) Huskinson, B.; Marshak, M. P.; Suh, C.; Er, S.; Gerhardt, M. R.; Galvin, C. J.; Chen, X.; Aspuru-Guzik, A.; Gordon, R. G.; Aziz, M. J. A Metal-Free Organic-Inorganic Aqueous Flow Battery. *Nature* **2014**, *505* (7482), 195−198.
(4) Lin, K.; Chen, Q.; Gerhardt, M. R.; Tong, L.; Kim, S. B.; Eisenach, L.; Valle, A. W.; Hardee, D.; Gordon, R. G.; Aziz, M. J.; Marshak, M. P. Alkaline Quinone Flow Battery. *Science* **2015**, *349* (6255), 1529−1532.
(5) Soloveichik, G. L. Flow Batteries: Current Status and Trends. *Chem. Rev.* **2015**, *115* (20), 11533−11558.
(6) Luo, J.; Wu, W.; Debruler, C.; Hu, B.; Hu, M.; Liu, T. L. A 1.51 V PH Neutral Redox Flow Battery towards Scalable Energy Storage. *J. Mater. Chem. A* **2019**, *7* (15), 9130−9136.
(7) Sevov, C. S.; Hendriks, K. H.; Sanford, M. S. Low-Potential Pyridinium Anolyte for Aqueous Redox Flow Batteries. *J. Phys. Chem. C* **2017**, *121* (44), 24376−24380.
(8) Sevov, C. S.; Hickey, D. P.; Cook, M. E.; Robinson, S. G.; Barnett, S.; Minteer, S. D.; Sigman, M. S.; Sanford, M. S. Physical Organic Approach to Persistent, Cyclable, Low-Potential Electrolytes for Flow Battery Applications. *J. Am. Chem. Soc.* **2017**, *139* (8), 2924−2927.
(9) Hendriks, K. H.; Robinson, S. G.; Braten, M. N.; Sevov, C. S.; Helms, B. A.; Sigman, M. S.; Minteer, S. D.; Sanford, M. S. High-Performance Oligomeric Catholytes for Effective Macromolecular Separation in Nonaqueous Redox Flow Batteries. *ACS Cent. Sci.* **2018**, *4* (2), 189−196.
(10) van Egmond, W. J.; Saakes, M.; Noor, I.; Porada, S.; Buisman, C. J. N.; Hamelers, H.V.M. Performance of an Environmentally Benign Acid Base Flow Battery at High Energy Density. *Int. J. Energy Res.* **2018**, *42* (4), 1524−1535.
(11) Sáez, A.; Montiel, V.; Aldaz, A. An Acid-Base Electrochemical Flow Battery as Energy Storage System. *Int. J. Hydrogen Energy* **2016**, *41* (40), 17801−17806.
(12) Kim, J.-H.; Lee, J.-H.; Maurya, S.; Shin, S.-H.; Lee, J.-Y.; Chang, I. S.; Moon, S.-H. Proof-of-Concept Experiments of an Acid-Base Junction Flow Battery by Reverse Bipolar Electrodialysis for an Energy Conversion System. *Electrochem. Commun.* **2016**, *72*, 157−161.
(13) Cohen, J. L.; Volpe, D. J.; Westly, D. A.; Pechenik, A.; Abruña, H. D. A Dual Electrolyte H_2/O_2 Planar Membraneless Microchannel Fuel Cell System with Open Circuit Potentials in Excess of 1.4 V. *Langmuir* **2005**, *21* (8), 3544−3550.
(14) Chen, B.; Leung, D. Y. C.; Xuan, J.; Wang, H. A Mixed-pH Dual-Electrolyte Microfluidic Aluminum-Air Cell with High Performance. *Appl. Energy* **2017**, *185*, 1303−1308.
(15) McDonald, M. B.; Ardo, S.; Lewis, N. S.; Freund, M. S. Use of Bipolar Membranes for Maintaining Steady-State pH Gradients in Membrane-Supported, Solar-Driven Water Splitting. *ChemSusChem* **2014**, *7* (11), 3021−3027.
(16) Giesbrecht, P. K.; Freund, M. S. Recent Advances in Bipolar Membrane Design and Applications. *Chem. Mater.* **2020**, *32* (19), 8060−8090.
(17) Yan, Z.; Zhu, L.; Li, Y. C.; Wycisk, R. J.; Pintauro, P. N.; Hickner, M. A.; Mallouk, T. E. The Balance of Electric Field and Interfacial Catalysis in Promoting Water Dissociation in Bipolar Membranes. *Energy Environ. Sci.* **2018**, *11* (8), 2235−2245.
(18) Wang, Z.; Parrondo, J.; He, C.; Sankarasubramanian, S.; Ramani, V. Efficient PH-Gradient-Enabled Microscale Bipolar Interfaces in Direct Borohydride Fuel Cells. *Nat. Energy* **2019**, *4* (4), 281−289.
(19) Mota, N. D.; Finkelstein, D. A.; Kirtland, J. D.; Rodriguez, C. A.; Stroock, A. D.; Abruña, H. D. Membraneless, Room-Temperature, Direct Borohydride/Cerium Fuel Cell with Power Density of Over 0.25 W/cm^2. *J. Am. Chem. Soc.* **2012**, *134* (14), 6076−6079.
(20) Ünlü, M.; Zhou, J.; Kohl, P. A. Hybrid Anion and Proton Exchange Membrane Fuel Cells. *J. Phys. Chem. C* **2009**, *113* (26), 11416−11423.
(21) Grew, K. N.; McClure, J. P.; Chu, D.; Kohl, P. A.; Ahlfield, J. M. Understanding Transport at the Acid-Alkaline Interface of Bipolar Membranes. *J. Electrochem. Soc.* **2016**, *163* (14), F1572−F1587.
(22) Vargas-Barbosa, N. M.; Geise, G. M.; Hickner, M. A.; Mallouk, T. E. Assessing the Utility of Bipolar Membranes for Use in Photoelectrochemical Water-Splitting Cells. *ChemSusChem* **2014**, *7* (11), 3017−3020.
(23) Luo, J.; Vermaas, D. A.; Bi, D.; Hagfeldt, A.; Smith, W. A.; Grätzel, M. Bipolar Membrane-Assisted Solar Water Splitting in Optimal PH. *Adv. Energy Mater.* **2016**, *6* (13), 1600100.
(24) Sun, K.; Liu, R.; Chen, Y.; Verlage, E.; Lewis, N. S.; Xiang, C. A Stabilized, Intrinsically Safe, 10% Efficient, Solar-Driven Water-Splitting Cell Incorporating Earth-Abundant Electrocatalysts with Steady-State PH Gradients and Product Separation Enabled by a Bipolar Membrane. *Adv. Energy Mater.* **2016**, *6* (13), 1600379.
(25) Xia, J.; Eigenberger, G.; Strathmann, H.; Nieken, U. Flow Battery Based on Reverse Electrodialysis with Bipolar Membranes: Single Cell Experiments. *J. Membr. Sci.* **2018**, *565*, 157−168.
(26) Oener, S. Z.; Foster, M. J.; Boettcher, S. W. Accelerating Water Dissociation in Bipolar Membranes and for Electrocatalysis. *Science* **2020**, *369* (6507), 1099−1103.
(27) Nikonenko, V. V.; Kozmai, A. E. Electrical Equivalent Circuit of an Ion-Exchange Membrane System. *Electrochim. Acta* **2011**, *56* (3), 1262−1269.
(28) Mareev, S. A.; Evdochenko, E.; Wessling, M.; Kozaderova, O. A.; Niftaliev, S. I.; Pismenskaya, N. D.; Nikonenko, V. V. A Comprehensive Mathematical Model of Water Splitting in Bipolar Membranes: Impact of the Spatial Distribution of Fixed Charges and Catalyst at Bipolar Junction. *J. Membr. Sci.* **2020**, *603*, 118010.
(29) Geissler, P. L. Autoionization in Liquid Water. *Science* **2001**, *291* (5511), 2121−2124.
(30) Hassanali, A.; Prakash, M. K.; Eshet, H.; Parrinello, M. On the Recombination of Hydronium and Hydroxide Ions in Water. *Proc. Natl. Acad. Sci. U. S. A.* **2011**, *108* (51), 20410−20415.
(31) Janoschka, T.; Martin, N.; Hager, M. D.; Schubert, U. S. An Aqueous Redox-Flow Battery with High Capacity and Power: The TEMPTMA/MV System. *Angew. Chem., Int. Ed.* **2016**, *55* (46), 14427−14430.
(32) Nutting, J. E.; Rafiee, M.; Stahl, S. S. Tetramethylpiperidine *N*-Oxyl (TEMPO), Phthalimide *N*-Oxyl (PINO), and Related *N*-Oxyl Species: Electrochemical Properties and Their Use in Electrocatalytic Reactions. *Chem. Rev.* **2018**, *118* (9), 4834−4885.
(33) Liu, Y.; Goulet, M.-A.; Tong, L.; Liu, Y.; Ji, Y.; Wu, L.; Gordon, R. G.; Aziz, M. J.; Yang, Z.; Xu, T. A Long-Lifetime All-Organic Aqueous Flow Battery Utilizing TMAP-TEMPO Radical. *Chem.* **2019**, *5* (7), 1861−1870.
(34) Chen, Y.; Wrubel, J. A.; Klein, W. E.; Kabir, S.; Smith, W. A.; Neyerlin, K. C.; Deutsch, T. G. High-Performance Bipolar Membrane Development for Improved Water Dissociation. *ACS Appl. Polym. Mater.* **2020**, *2* (11), 4559−4569.

https://doi.org/10.1021/acscentsci.1c00217
ACS Cent. Sci. 2021, 7, 1028−1035

(35) Gu, S.; Gong, K.; Yan, E. Z.; Yan, Y. A Multiple Ion-Exchange Membrane Design for Redox Flow Batteries. *Energy Environ. Sci.* **2014**, *7* (9), 2986−2998.
(36) Gong, K.; Ma, X.; Conforti, K. M.; Kuttler, K. J.; Grunewald, J. B.; Yeager, K. L.; Bazant, M. Z.; Gu, S.; Yan, Y. A Zinc-Iron Redox-Flow Battery under $100 per KWh of System Capital Cost. *Energy Environ. Sci.* **2015**, *8* (10), 2941−2945.
(37) Blommaert, M. A.; Verdonk, J. A. H.; Blommaert, H. C. B.; Smith, W. A.; Vermaas, D. A. Reduced Ion Crossover in Bipolar Membrane Electrolysis *via* Increased Current Density, Molecular Size, and Valence. *ACS Appl. Energy Mater.* **2020**, *3* (6), 5804−5812.
(38) Baran, M. J.; Braten, M. N.; Sahu, S.; Baskin, A.; Meckler, S. M.; Li, L.; Maserati, L.; Carrington, M. E.; Chiang, Y.-M.; Prendergast, D.; Helms, B. A. Design Rules for Membranes from Polymers of Intrinsic Microporosity for Crossover-Free Aqueous Electrochemical Devices. *Joule* **2019**, *3* (12), 2968−2985.
(39) Tan, R.; Wang, A.; Malpass-Evans, R.; Williams, R.; Zhao, E. W.; Liu, T.; Ye, C.; Zhou, X.; Darwich, B. P.; Fan, Z.; Turcani, L.; Jackson, E.; Chen, L.; Chong, S. Y.; Li, T.; Jelfs, K. E.; Cooper, A. I.; Brandon, N. P.; Grey, C. P.; McKeown, N. B.; Song, Q. Hydrophilic Microporous Membranes for Selective Ion Separation and Flow-Battery Energy Storage. *Nat. Mater.* **2020**, *19* (2), 195−202.
(40) Zuo, P.; Li, Y.; Wang, A.; Tan, R.; Liu, Y.; Liang, X.; Sheng, F.; Tang, G.; Ge, L.; Wu, L.; Song, Q.; McKeown, N. B.; Yang, Z.; Xu, T. Sulfonated Microporous Polymer Membranes with Fast and Selective Ion Transport for Electrochemical Energy Conversion and Storage. *Angew. Chem., Int. Ed.* **2020**, *59* (24), 9564−9573.

https://doi.org/10.1021/acscentsci.1c00217
ACS Cent. Sci. 2021, 7, 1028−1035